

Divergent Impact of Actin Isoforms on Division of Epithelial Cells

G. S. Shagieva¹, I. B. Alieva^{1,2,a*}, C. Chaponnier³, and V. B. Dugina¹

¹Belozersky Institute of Physico-Chemical Biology, Lomonosov Moscow State University, 119992 Moscow, Russia

²Federal Research and Clinical Center of Physical-Chemical Medicine
of the Federal Medical Biological Agency, 119435 Moscow, Russia

³Department of Pathology and Immunology, Faculty of Medicine, University of Geneva, 1205 Geneva, Switzerland

^ae-mail: irina_alieva@belozersky.msu.ru

Received June 23, 2020

Revised July 22, 2020

Accepted July 25, 2020

Abstract—We investigated distribution and functions of beta- and gamma-cytoplasmic actins (CYAs) at different stages of non-neoplastic epithelial cell division using laser scanning microscopy (LSM). Here, we demonstrated that beta- and gamma-CYAs are spatially segregated in the early prophase, anaphase, telophase, and cytokinesis. Small interfering RNA (siRNA) experiments revealed that in both beta-CYA- and gamma-CYA-depleted cells, the number of cells was significantly reduced compared with the siRNA controls. Beta-CYA depletion resulted in an enlargement of the cell area in metaphase and high percentage of polynuclear cells compared with the siRNA control, indicating a potential failure of cytokinesis. Gamma-CYA depletion resulted in a reduced percentage of mitotic cells. We also observed the interdependence between the actin isoforms and the microtubule system in mitosis: (i) a decrease in the gamma-CYA led to impaired mitotic spindle organization; (ii) suppression of tubulin polymerization caused impaired beta-CYA reorganization, as incubation with colcemid blocked the transfer of short beta-actin polymers from the basal to the cortical compartment. We conclude that both actin isoforms are essential for proper cell division, but each isoform has its own specific functional role in this process.

DOI: 10.1134/S0006297920090072

Keywords: cytoplasmic actin, mitosis, microtubules, cell division

INTRODUCTION

Actin and its regulatory proteins are critically important in the cell division. The actin cytoskeleton of epithelial cells consists of two cytoplasmic actin (CYA) isoforms and numerous actin binding proteins providing different cytoskeleton structures. Beta- and gamma-CYAs are expressed almost in all human cells in different proportions and differ only by four amino acids located at positions 1, 2, 3, and 9 at the N-terminus [1]. We have previously shown that beta- and gamma-CYAs display distinct distribution and functions in the fibroblasts and epithelial cells. Beta-CYA predominantly forms contractile stress fibers, whereas gamma-CYA is organized in a fine apical meshwork of actin filaments throughout the cell [2, 3].

During transition to cell division, all cytoskeletal components undergo significant changes. Interaction of

actin and microtubules is important for the regulation of cell shape and polarity during cell division from the entry into the prophase until the end of cytokinesis. Under the term *cell division*, we mean the entire M phase of the cell cycle including mitosis (karyokinesis) and cytokinesis. The mechanisms of actin–microtubule crosstalk include different cytoskeletal regulators (Rho-GTPases, for example) and various physical interactions of filament systems (crosslinking, anchoring, and mechanical support) [4]. It is known that (i) interactions of actin filaments with the microtubules play an important role in the assembly and maintenance of the 3D cell structure and (ii) beta- and gamma-CYAs produce the opposite effect on the microtubule dynamics and organization [3]. Here, we attempted to reveal whether microtubules affect the functional activity of beta- or gamma-CYA structures, and vice versa, during the cell division in non-tumour epithelial HaCaT cells [5]. We used laser scanning microscopy (LSM), regulation of actin expression with small interfering RNAs (siRNAs), and chemical inhibitors that affect microtubule dynamics, to investigate

Abbreviations: CYA, cytoplasmic actin; LSM, laser scanning microscopy; siRNA, small interfering RNA.

* To whom correspondence should be addressed.

the distribution and functions of each CYA isoform at different stages of epithelial cell division.

MATERIALS AND METHODS

Cells, culturing conditions, and reagents. HaCaT cells are spontaneously immortalized *in vitro* keratinocytes from a surgical specimen of histologically normal human skin [5]. The HaCaT cell line was kindly provided by Lionel Fontao (Department of Dermatology, University Hospital of Geneva, Switzerland). The cells were maintained in Dulbecco's modified Eagle medium (DMEM; Gibco, Switzerland) with 5% fetal bovine serum (Seromed, Germany) and 5 mM glutamic acid (PanEco, Russia). For the experiments, the cells were cultured in plastic flasks at 37°C in 5% CO₂ until they reached a confluent monolayer and then plated onto glass coverslips for 3–8 h (37°C, 5% CO₂) to obtain separately located mitotic cells. One of the following inhibitors was added to the culture medium: (i) 25 μM blebbistatin (selective inhibitor of non-muscle myosin II; Biomol International, USA) for 4 h (37°C, 5% CO₂); (ii) 2 μM tubulin-stabilizing drug taxol (Paclitaxel; Sigma, USA) for 5 h (37°C, 5% CO₂); (iii) 0.1 μg/ml tubulin-destabilizing drug colcemid (Demecolcine; Sigma) for 1 h (37°C, 5% CO₂).

Antibodies. The following primary antibodies were used: anti-beta-CYA (mouse mAbs 4C2, IgG1, Bio-Rad; AC-74, IgG2a, Sigma), anti-gamma-CYA (mouse mAb 2A3, IgG2b, Bio-Rad; rabbit pAbs AAL20), anti-pan-actin (clone C4, Chemicon, USA), anti-α-tubulin (clone DM1A, IgG1, Sigma), rabbit antibodies against non-muscle myosin IIA (Sigma), mouse anti-Rac1 (mAb, IgG2b, BD Transduction, USA); and rabbit anti-Rho (mAb, Epitomics/Abcam, USA). All primary antibodies were used at a 1 : 100 dilution for microscopy. The following secondary antibodies were used: Alexa488-, Alexa594-, and Alexa647-conjugated goat anti-mouse IgG1, IgG2b, and IgG2a (Southern Biotechnology Associates Inc., USA). TRITC- or Cy-5-conjugated goat anti-rabbit antibodies (Jackson ImmunoResearch Laboratories Inc., USA). All secondary antibodies were used at a 1 : 500 dilution for cell staining. DRAQ5 (Biostatus, UK) and DAPI (Sigma) were applied for nuclear staining.

Western blot analysis. The cells were washed off from cultural plastic dishes and extracted with cold sample buffer [62.5 mM Tris-HCl, pH 6.8, 2% sodium dodecyl sulfate (SDS), 10% glycerin (v/v), 50 mM dithiothreitol, 0.01% bromophenol blue; protease and phosphatase inhibitors cocktail (Sigma)]. The lysates were separated in 10% SDS polyacrylamide gel and transferred onto polyvinylidene fluoride membrane (Amersham GE Healthcare, USA). After blocking the nonspecific binding with bovine serum albumin, the membranes were

incubated with primary specific antibodies. α-Tubulin was used as a loading control. Next, the membranes were incubated with horseradish peroxidase-conjugated secondary antibodies (Amersham GE Healthcare) at a dilution 1 : 30,000. The membranes were developed using the chemiluminescence technique with ECL reagents (Amersham GE Healthcare) according to the manufacturer's protocol. Chemiluminescence was detected with a photosensitive film. The resulting films were scanned and analyzed densitometrically with the ImageJ 1.37C Software (NIH, <http://rsb.info.nih.gov/ij/>). The difference in the relative amount of protein was estimated using the Mann-Whitney *U*-test based on the results of five independent experiments.

Immunofluorescence and confocal LSM. For immunofluorescent staining, the cells were cultured on glass coverslips, washed for 1 min with DMEM containing 20 mM HEPES at 37°C, and fixed for 15 min with 1% paraformaldehyde in the pre-warmed serum-free DMEM (with 20 mM HEPES) at room temperature.

Then, the cells were fixed/permeabilized with cold MeOH at -20°C for 5 min for antibody staining. The permeabilization/fixation conditions used in this study are crucial for better accessibility of the N-terminus of actin isoforms [2]. For immunofluorescence staining of RhoA and Rac1, the cells were fixed with 10% trichloroacetic acid (-20°C) for 15 min. Immunofluorescence was observed using a confocal microscope (LSM510, Zeiss, Germany) equipped with oil immersion objectives (Plan-Neofluar 63×/1.4 and Plan-Fluar 100×/1.45, Zeiss). The obtained images (single optical sections, ~1 μm) were processed with the Zeiss LSM Software for LSM510 (Zeiss). Cell area measurements were performed with the Zeiss LSM Software for LSM510 (Zeiss); the data were obtained from three independent experiments for at least 20 cells for each condition. Beta-CYA immunofluorescence (IF) intensity was analyzed with the ImageJ 1.37C Software using the "multi-point" tool in a single-color channel. Mean values of IF intensity for multiple measurements of 30 points per cortical region or cytosolic actin accumulations were obtained for each cell. The results are presented as mean for 10–15 cells ± standard error of the mean for each condition for two types of localization.

siRNA transfection. Used sequences of human beta-CYA (NM_001101) siRNAs and human gamma-CYA (NM_001614) siRNAs (Qiagen, Switzerland) are presented in the table.

The cells were transfected with 50–100 nM siRNA smart pools using Lipofectamine 2000 (Invitrogen, USA). The transfection efficiency (≥ 90%) was estimated using BLOCK-iT™ (Invitrogen). HaCaT cells transfected with scrambled control/beta-CYA siRNA/gamma-CYA siRNA were analyzed on day 3 after transfection. Quantification of cell populations after CYA depletion was performed by analyzing the total number of cells in the

siRNA sequences	
siRNA	Sequence (5'-3')
Beta-CYA siRNA1	AATGAAGATCAAGATCATTGC
Beta-CYA siRNA2	TAGCATTGCTTCGTGTAAT
Beta-CYA siRNA3	CAAATATGAGATGCATTGTTA
Gamma-CYA siRNA1	AAGAGATGCCCGCGCTGGTCA
Gamma-CYA siRNA2	CAGCAACACGTCATTGTGTA

suspension after detachment from the substrate. The proportion of multinucleated cells was estimated as the count of multinucleated cells among random 100 cells for each experimental condition; the proportion of mitoses was calculated as the number of mitotic cells per random 100 cells of the population for each experimental condition.

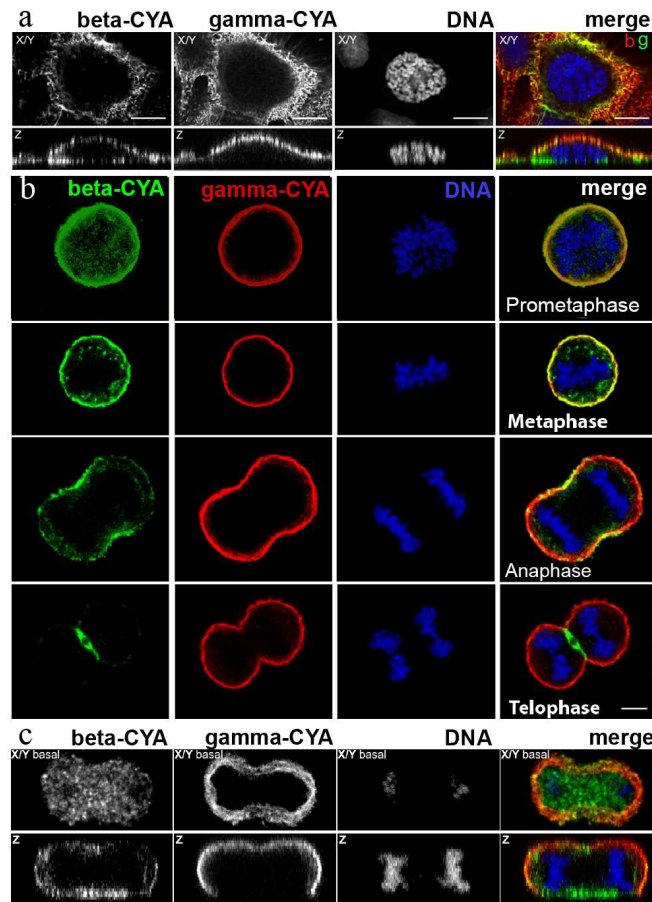


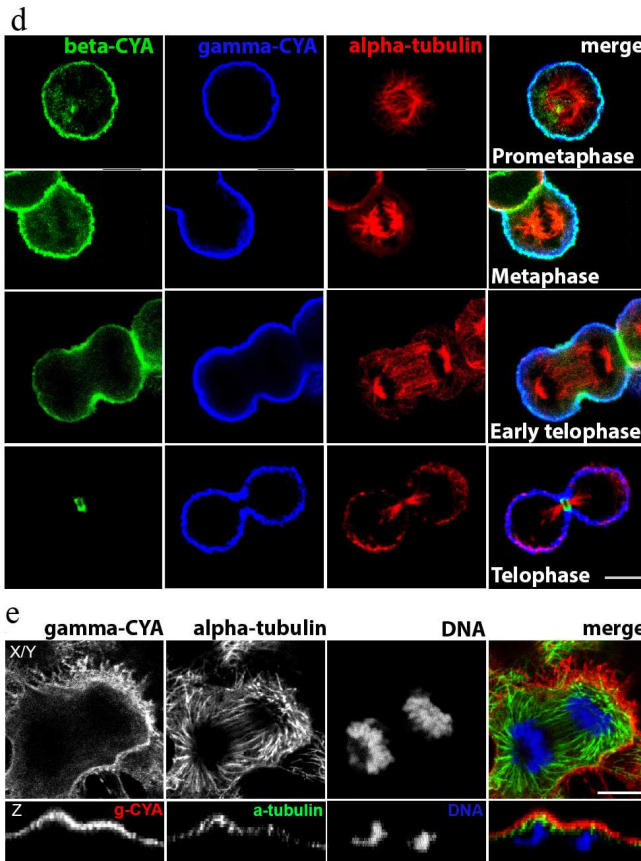
Fig. 1. LSM. a) Distribution of CYAs in early prophase in HaCaT cells; X/Y and Z sections; beta-CYA (green), gamma-CYA (red), DNA (blue) on the merged image. b) Distribution of CYAs during the mitotic phases (prophase, metaphase, anaphase, telophase) and cytokinesis in HaCaT cells; beta-CYA (green), gamma-CYA (red), DNA (blue). c) CYAs at the basal optical level in mitotic HaCaT cell; beta-CYA (green), gamma-CYA (red), DNA (blue) on the merged image. d) Distribution of CYAs and tubulin during mitosis (prometaphase, metaphase, early telophase, telophase) and cytokinesis in HaCaT cells: beta-CYA (green), gamma-CYA (blue), alpha-tubulin (red). e) Gamma-CYA (red), alpha-tubulin (green) and DNA (blue) in anaphase in HaCaT on merged image. Upper row, X/Y section; lower row, Z section. Scale bars: 5 μ m. (Color versions of Figs. 1-4 are available in the online version of the article and can be accessed at: <https://www.springer.com/journal/10541>)

Statistical analysis. The results are presented as mean \pm standard error of the mean of at least three independent experiments. The differences between the groups were analyzed by the Mann–Whitney *U*-test. The values of $p < 0.001$ (***) $, p < 0.01$ (**), and $p < 0.05$ (*) were considered as statistically significant.

RESULTS

Subcellular location of beta- and gamma-CYAs at different phases of cell division. Triple immunofluorescence analysis of beta- and gamma-CYAs, as well as alpha-tubulin, during mitotic phases and cytokinesis in HaCaT cells allowed to establish that the two CYAs are specifically distributed in the dividing epithelial cells.

In early prophase cells, the CYAs were segregated similar to the interphase cells [2]: beta-CYA formed ven-



tral fibers and gamma-CYA was organized in a dorsal network (Fig. 1a). The measurements of the beta-CYA IF intensity in the prometaphase revealed only a slight predominance of beta-CYA in the cortex (158.43 ± 16.9) compared with the cytoplasm (132.6 ± 15.8). In metaphase, both CYAs enriched the cortical compartment (Fig. 1, b and d). In anaphase, beta-CYA was recruited to the equatorial cortex where it concentrated in the contractile ring during telophase and cytokinesis (Fig. 1, b and d). Beta-CYA bundles were also located ventrally in the zone of cell-substrate contacts during the cell division (Fig. 1, a and c). Gamma-CYA formed the cortical network during all mitotic phases and cytokinesis (Fig. 1). The distribution of CYAs and tubulin during the mitotic phases and cytokinesis in HaCaT cells is shown in Fig. 1, c and d.

Effect of blebbistatin on CYA distribution. Location of RhoA and Rac1 during cytokinesis. Blebbistatin is an inhibitor of non-muscle myosin II which blocks myosin II in the actin-detached state [6]. We treated epithelial HaCaT cells with blebbistatin to reveal its effect on CYA distribution. In most animal cells, cytokinesis begins in anaphase and ends shortly after telophase [7]. Blebbistatin inhibits contraction of the cleavage furrow without disrupting mitosis [8]. Double immunofluorescent staining showed that in anaphase and telophase of blebbistatin-treated cells, the concentration of beta-CYAs' accumulation in the equatorial region was attenuated compared with the control (Fig. 2, a and b), while the gamma-CYA network remained unchanged (data not shown).

Typical Rho GTPases are well-known regulators of the actin and microtubule cytoskeleton organization [9]. To reveal a possible specificity of Rho GTPases to the CYA isoforms, we studied the location of RhoA and Rac1 in telophase HaCaT cells. The contractile ring assembly requires spatio-temporal control via small GTPase signaling [10]. We detected RhoA recruitment to the equatorial region and contractile ring in telophase/cytokinesis, similarly to beta-CYA, but not gamma-CYA (Fig. 2c). Another Rho-GTPase, Rac1, was distributed evenly in the cytoplasm with slight concentration in the polar cortex in telophase cells, where it overlapped with gamma-CYA (Fig. 2d).

Depletion of beta- or gamma-CYAs suppressed epithelial cell division and induced distinct mitosis defects. Considering segregation of actin isoforms in the mitotic HaCaT cells, we transfected the cells with siRNAs for beta- or gamma-CYAs to evaluate the contribution of CYAs to the mitosis progression. The downregulation of beta-CYA by the specific siRNA 72 h post-transfection was $37.7 \pm 4.3\%$; it was accompanied with slight increase in gamma-CYA amount ($9.5 \pm 5.2\%$). The reduction of gamma-CYA by the specific siRNA was $35.5 \pm 5.8\%$, whereas the concentration of beta-CYA did not increase significantly (Fig. 3a).

The downregulation of CYAs in HaCaT cells led to significant alterations in cell proliferation *in vitro*; however, the silencing of different CYA isoforms affected the mitotic processes diversely. In both beta- and gamma-CYA depleted cell populations, the number of cells on day 3 after transfection was lower compared with the scrambled controls: $36.7 \pm 2.53\%$ for beta-CYA siRNA and $47.5 \pm 8.2\%$ for gamma-CYA siRNA (Fig. 3b). In the beta-CYA-depleted cells, we observed an increase in the cell area in the metaphase, failure of cytokinesis, and appearance of polynuclear cells. The cell area in the metaphase for cells transfected with the scrambled siRNA was $214,149 \pm 31,009 \mu\text{m}^2$, beta-CYA siRNA – $496,112 \pm 68,265 \mu\text{m}^2$, gamma-CYA siRNA – $157,043 \pm 14,652 \mu\text{m}^2$. The downregulation of beta-CYA resulted in a high percentage of binuclear cells ($29 \pm 2\%, p < 0.001$) compared with 2% in both scrambled control-transfected and gamma-CYA-depleted cells (Fig. 3c). In gamma-CYA-depleted HaCaT cells, the proportion of mitotic cells decreased 3.4 times on the second post-transfection day and 2.2 times on the third post-transfection day compared with the scrambled siRNA-transfected cells. In beta-CYA-depleted cells, the content of mitotic cells was 1.8 times less on the second day after transfection compared with the control and was the same as in the scramble siRNA-transfected cells on the third day. We also revealed a delay in the spindle formation (data not shown), cortical blebbing, and a variety of nuclear deformations (Fig. 3d) including strong asymmetry of chromosome organization, nuclear fragmentation, and small nuclei, in the gamma-CYA depleted cells (data not shown).

During the interphase, the microtubules are organized into a 3D radial system and their plus-ends terminate close to the actin cortex [3]. We found that spindle and astral microtubules were normally organized in the control and beta-CYA-depleted mitotic cells; however, gamma-CYA downregulation led to the disorganization of the microtubule network (Fig. 3d).

Interrelationships between microtubules and CYAs. Interaction of actin filaments with the microtubules play an important role in the assembly and maintenance of the cell 3D structure. Taxol, which is a plant-derived antitumor drug, is a microtubule-stabilizing agent. Taxol binds stoichiometrically and specifically to the beta-tubulin subunit in tubulin dimers, resulting in stable microtubules [11]. Stabilization of the microtubules by taxol didn't disrupt the cortical localization of beta- and gamma-CYAs in metaphase, and the connection of microtubules with the cortex was maintained (Fig. 4a). Colcemid, which is a derivative of colchicine, has the opposite effect: it binds tubulin and inhibits microtubule polymerization and mitotic spindle formation [12, 13]. We used colcemid treatment to block the cells in metaphase. After colcemid was removed, the microtubule repolymerized and formed the mitotic spindle. One hour after the drug removal,

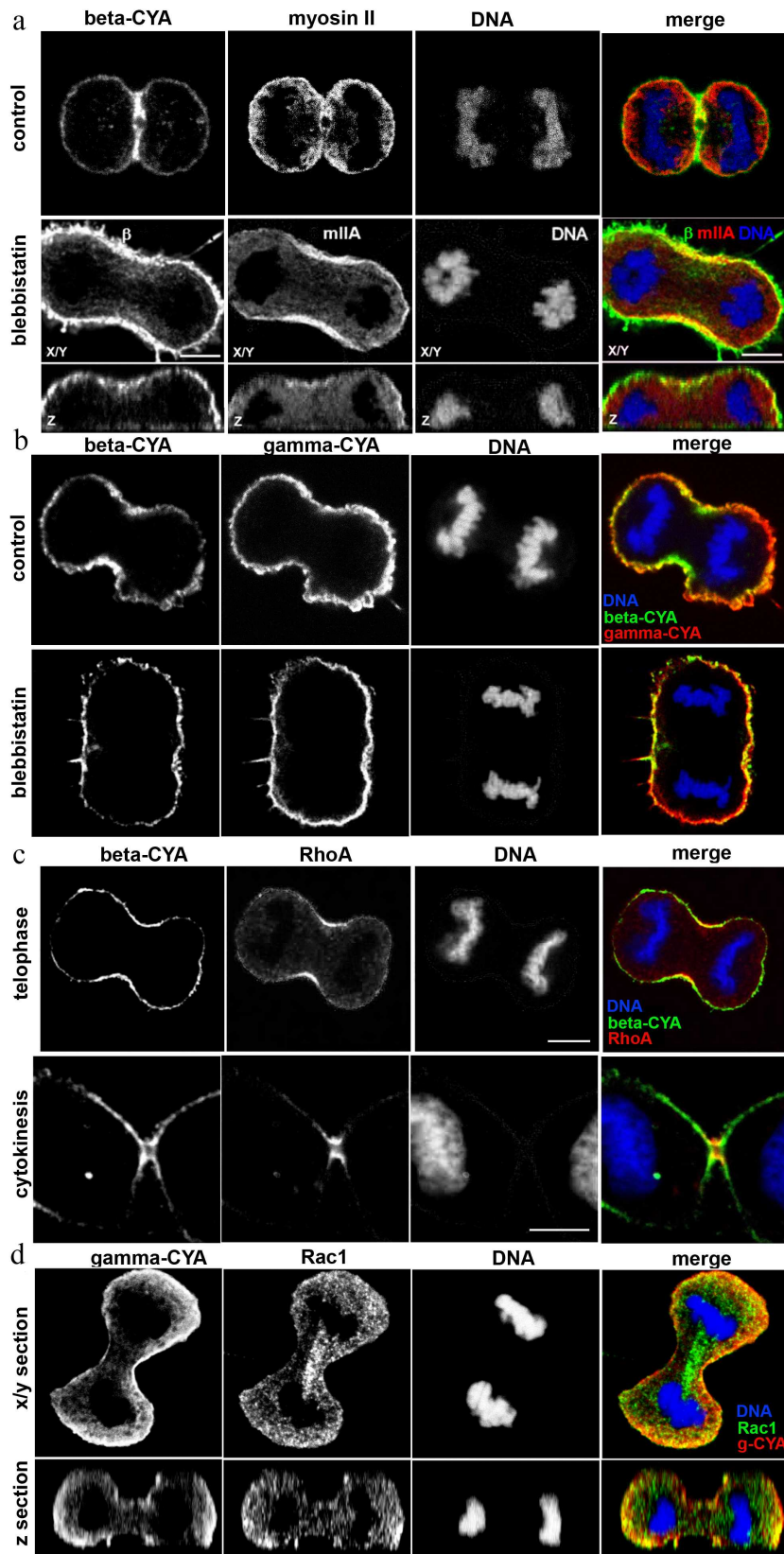


Fig. 2. LSM. a) Beta-CYA (green), myosin IIA (red), and DNA (blue) in the blebbistatin-treated HaCaT cells in telophase/cytokinesis. b) Beta-CYA (green), gamma-CYA (red), and DNA (blue) in the blebbistatin-treated HaCaT cells in anaphase/cytokinesis. c) RhoA (red), beta-CYA (green), and DNA (blue) during telophase/cytokinesis in HaCaT cells. d) Gamma-CYA (red), Rac1 (green), and DNA (blue) during the telophase in HaCaT cells. X/Y and Z sections. Scale bar: 5 μm.

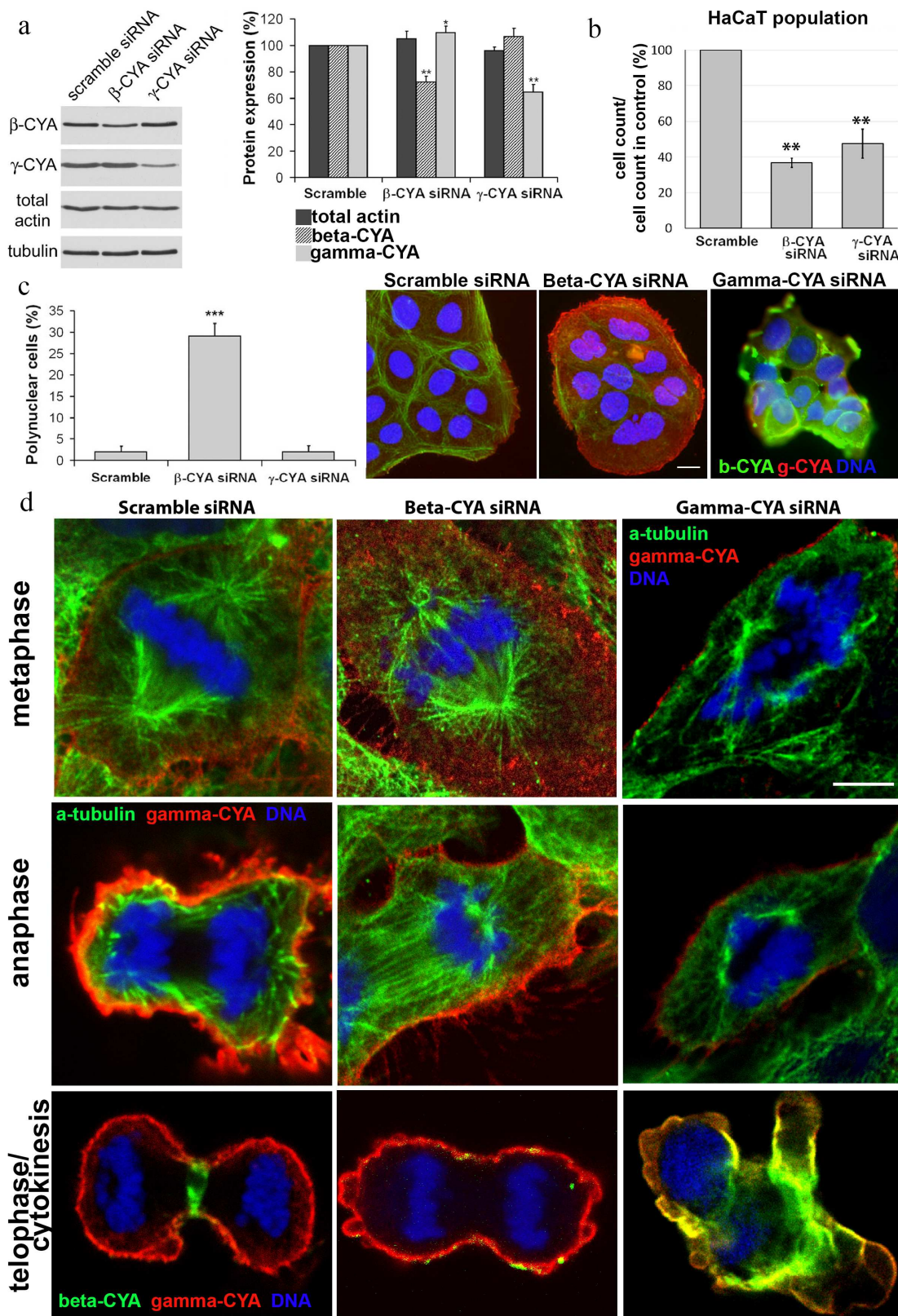


Fig. 3. LSM. a) Depletion of beta- and gamma-CYAs with siRNAs. Western blot. b) Reduction of the HaCaT cell population induced by beta- or gamma-CYA siRNAs. c) Increased rate of polynuclear cells after beta-CYA depletion compared with the scrambled control-transfected and gamma-CYA depleted cells. Scale bar: 10 μ m. d) Metaphase, anaphase and telophase/cytokinesis in HaCaT cells transfected with beta- or gamma-CYA siRNAs. Two upper panels: gamma-CYA (red), alpha-tubulin (green), DNA (blue). Lower panel: gamma-CYA (red), beta-CYA (green), DNA (blue). Scale bar: 5 μ m.

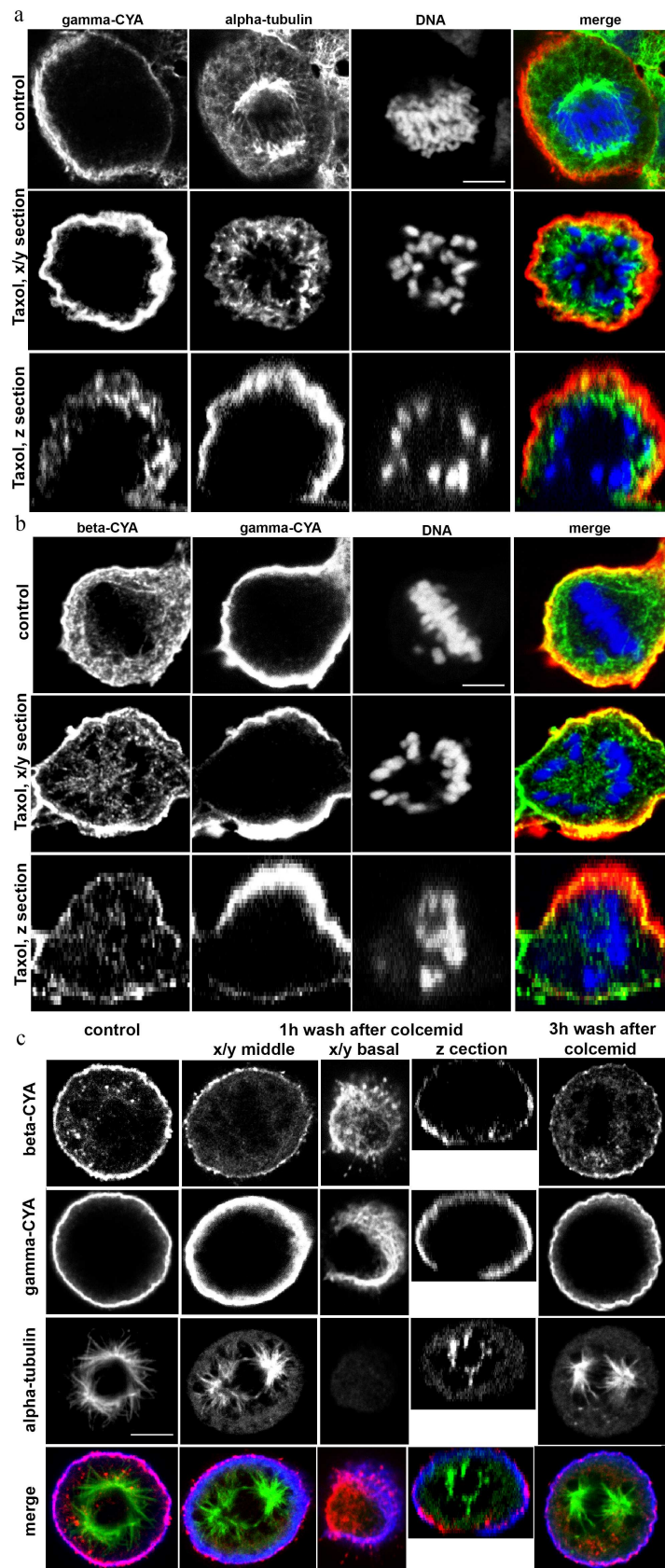


Fig. 4. LSM. a) The effects of taxol treatment on HaCaT cells in mitosis: alpha-tubulin (green); gamma-CYA (red); DNA (blue). b) Beta-CYA (green), gamma-CYA (red), and DNA (blue) in taxol-treated HaCaT cells. c) CYAs and alpha-tubulin in the colcemid-treated HaCaT cells 1 and 3 h after the drug removal compared with the control: alpha-tubulin (green); beta-CYA (red); gamma-CYA (blue). Scale bars: 5 μ m.

small beta-CYA fibers were revealed at the basal level of the cell and near the spindle microtubules (Fig. 4b). Three hours after colcemid removal, beta-CYA was concentrated in the cortex in addition to small fibers with cytoplasmic and basal location. Gamma-CYA location was not affected by colcemid (Fig. 4b). To analyze the distribution of beta-CYA after colcemid treatment/wash-off and taxol treatment, we measured beta-CYA IF intensity in the cortex and the cytoplasm. In the control metaphase cells, the IF intensity of beta-CYA was $237,417 \pm 12,257$ in the cortex and $63,861 \pm 18,317$ in the cytoplasm. In the colcemid-treated cells 3 h after the removal of the drug, the intensity of beta-CYA IF was $136,259 \pm 12,836$ in the cell cortex and $92,308 \pm 22,885$ in the cytoplasm. In the taxol-treated (5 h) cells, the intensity beta-CYA IF was $198,15 \pm 14.74$ in the cortex and $153,24 \pm 20.48$ in the cytoplasm.

DISCUSSION

In our work, we revealed distinct localization of CYAs structures at the different stages of mitotic division, including cytokinesis, in epithelial HaCaT cells.

Gamma-CYA was organized in the cortical network during all the mitotic phases and cytokinesis and did not participate in the contractile ring formation. The decreased expression of gamma-CYA induced cortical blebbing and deformations in the shape of the mitotic cells. Previously, it was shown that microinjections of antibodies to gamma-CYA (but not beta-CYA) lead to significant disturbances in the shape of oocytes, deformations of the cortex, and blebbing [14]. Beta-CYA formed basal fibers in the early prophase, accumulated in the cortical compartment in metaphase, was recruited to the equatorial region in anaphase, and formed the contractile ring in telophase and cytokinesis. Participation of beta-CYA in the contractile ring formation is consistent with our previous data [2] and observation of mitosis in SH-EP and HeLa cancer cells [15, 16]. Beta-CYA bundles were also detected in the basal cell level; we suggest that they provided cell adhesion to the substrate during mitosis.

There are several key events during mitosis when actin involvement is crucial. One of the mitotic events in which actin network plays an important role is the separation of centrosomes. Actin cytoskeleton is required for spindle formation [17]. Disruption of actin and myosin II structures and depolymerization of actin filaments causes failure in the centrosome separation and proper spindle assembly [18–20]. A growing body of evidence suggests that actin is involved not only in the movement and positioning of the spindle during meiotic division, but also protects oocytes from the chromosome segregation errors resulting in aneuploidy [21]. We have previously demonstrated a specific interaction between microtubules and cytoplasmic gamma-CYA (but not beta-CYA), mediated

by the plus-terminal microtubule protein EB1 in tumour epithelial cell lines [3]. In this work, we showed that even a moderate decrease of gamma-, but not beta-CYA, caused disturbances in the structure of mitotic spindle in epithelial cells. Previously, it was demonstrated that the partial depletion of gamma-CYA and not beta-CYA promotes centrosome amplification in cancer cells and causes a significant delay in prometaphase/metaphase. Such prolonged prometaphase/metaphase arrest was accompanied by mitotic defects associated with chromosome aggregation and correlated with increased mitotic spindle abnormalities in the gamma-CYA-depleted cells [15]. Contrariwise, microtubule organization can influence the microfilament system. Our data suggest that the transport of beta-actin from the basal cell level to the cortex depends on the functional microtubule system.

At the end of mitosis, actin rearranges and forms the contractile ring, which is essential for separation of daughter cells during cytokinesis. The contractile ring is a system of actin and myosin filaments directed by the RhoA GTPase; it generates the force required to deform the plasma membrane and to drive cytokinetic furrow ingression [22]. Myosin II inhibitor blebbistatin decreased the concentration of beta-CYA in the equatorial zone but did not disturb the gamma-CYA network in anaphase of HaCaT cells. Beta-CYA-depleted cells exhibited impaired cytokinesis, resulting in a high percentage of polynuclear cells. Recently, it was shown that stabilization and organization of the cytokinetic furrow is specifically provided by the beta-CYA filament assembly at the site of cytokinesis [16]. It is also noteworthy that beta-CYA filaments are assembled directly at the furrow by the anillin-dependent pathway. Anillin is required to maintain active myosin in the equatorial plane during cytokinesis, suggesting it functions as a scaffold protein to link RhoA with the ring components – actin and myosin [23, 24]. In anillin-depleted asynchronous population of HeLa cells after 24 h of RNAi treatment, 40–50% of cells are binucleated [25].

The formation of stress fibers and lamellipodia is regulated by the small GTP-binding proteins RhoA and Rac1, respectively [26]. The assembly and the operation of the contractile ring are controlled by RhoA GTPase [27]. Accumulation of RhoA at the equator prior to the cytokinesis was reported previously [25, 28]. Here, we observed a similar accumulation of RhoA in mitotic non-tumour HaCaT cells. Rho GTPase activates Rho-associated protein kinase (ROCK), which, in turn, increases the contractile force of actin cytoskeleton through phosphorylation of the myosin light chain [29]. The selective inhibitor of ROCK, Y-27632, induced disorganization of beta-CYA bundles, without disturbing the gamma-CYA microfilament network [2]. Taken together, these data suggest that RhoA is required for beta-CYA (but not gamma-CYA) regulation.

Rho GTPases transmit signals from the membrane receptors to the cytoskeleton and cell adhesions. Small

GTPase Rac1 promotes actin assembly at the cell periphery to produce lamellipodia and membrane ruffles [30]. The inhibitor of Rac1 GDP/GTP exchange activity NSC23766 suppressed protrusions, induced the loss of lamella and lamellipodia, disturbed the gamma-CYA network, and enhanced formation of beta- and gamma-CYA stress fibers in the interphase cells [2]. In mammalian oocytes, Rac1 regulates meiotic spindle stability and anchoring to the cortex [31]. In telophase HaCaT cells, Rac1 was distributed evenly in the cytoplasm with slight concentration at the polar periphery together with gamma-CYA. Considering our previous observations [32, 33], we propose that Rac1 influences gamma-CYA network via ERK1/2 and regulates locomotion at the leading edge of daughter cells in cytokinesis.

Here, we demonstrated for the first time different distribution of CYA isoforms at all mitotic phases and functional crosstalk between beta-CYA, gamma-CYA, and microtubules in non-tumour epithelial cells. We suggest that both CYAs are essential for proper cell division, but each isoform has a specific function, which requires further study in various cell models.

Funding. This work was supported by the Russian Foundation for Basic Research (projects nos. 18-29-09082, 18-34-00047) and by the Lomonosov Moscow State University development program (PNR 5.13).

Ethics declarations. The authors declare no conflict of interest in financial or any other sphere. This article does not contain any studies with human participants or animals performed by any of the authors.

REFERENCES

- Ampe, C., and Van Troys, M. (2017) Mammalian actins: isoform-specific functions and diseases, *Handb. Exp. Pharmacol.*, **235**, 1-37, doi: 10.1007/164_2016_43.
- Dugina, V., Zwaenepoel, I., Gabbiani, G., Clément, S., Chaponnier, C., Clément, S., and Chaponnier, C. (2009) Beta and gamma-cytoplasmic actins display distinct distribution and functional diversity, *J. Cell Sci.*, **122**, 2980-2988, doi: 10.1242/jcs.041970.
- Dugina, V., Alieva, I., Khromova, N., Kireev, I., Gunning, P. W., and Kopnin, P. (2016) Interaction of microtubules with the actin cytoskeleton via cross-talk of EB1-containing +TIPs and γ -actin in epithelial cells, *Oncotarget*, **7**, 72699-72715, doi: 10.18632/oncotarget.12236.
- Dogterom, M., and Koenderink, G. H. (2019) Actin-microtubule crosstalk in cell biology, *Nat. Rev. Mol. Cell Biol.*, **20**, 38-54, doi: 10.1038/s41580-018-0067-1.
- Boukamp, P., Petrussevska, R. T., Breitkreutz, D., Hornung, J., Markham, A., and Fusenig, N. E. (1988) Normal keratinization in a spontaneously immortalized aneuploid human keratinocyte cell line, *J. Cell Biol.*, **106**, 761-771, doi: 10.1083/jcb.106.3.761.
- Kovács, M., Tóth, J., Hetényi, C., Málnási-Csizmadia, A., and Sellers, J. R. (2004) Mechanism of blebbistatin inhibition of myosin II, *J. Biol. Chem.*, **279**, 35557-35563, doi: 10.1074/jbc.M405319200.
- Alberts, B., Johnson, A., Lewis, J., Raff, M., Roberts, K., and Walter, P. (2008) Cytokinesis, in *Molecular Biology of the Cell*, 5th Edn., Garland Science, New York, pp. 1092-1093.
- Straight, A. F., Cheung, A., Limouze, J., Chen, I., Westwood, N. J., Sellers, J. R., and Mitchison, T. J. (2003) Dissecting temporal and spatial control of cytokinesis with a myosin II inhibitor, *Science*, **299**, 1743-1747, doi: 10.1126/science.1081412.
- Etienne-Manneville, S., and Hall, A. (2002) Rho GTPases in cell biology, *Nature*, **420**, 629-635, doi: 10.1038/nature01148.
- Bement, W. M., Miller, A. L., and Von Dassow, G. (2006) Rho GTPase activity zones and transient contractile arrays, *BioEssays*, **28**, 983-993, doi: 10.1002/bies.20477.
- Xiao, H., Verdier-Pinard, P., Fernandez-Fuentes, N., Burd, B., Angeletti, R., Fiser, A., Horwitz, S. B., and Orr, G. A. (2006) Insights into the mechanism of microtubule stabilization by taxol, *Proc. Natl. Acad. Sci. USA*, **103**, 10166-10173, doi: 10.1073/pnas.0603704103.
- Borisy, G. G., and Taylor, E. W. (1967) The mechanism of action of colchicine. Colchicine binding to sea urchin eggs and the mitotic apparatus, *J. Cell Biol.*, **34**, 535-548, doi: 10.1083/jcb.34.2.535.
- Borisy, G. G., and Taylor, E. W. (1967) The mechanism of action of colchicine. Binding of colchicine-3H to cellular protein, *J. Cell Biol.*, **34**, 525-533, doi: 10.1083/jcb.34.2.525.
- Brockmann, C., Huarte, J., Dugina, V., Challet, L., Rey, E., Conne, B., Swetloff, A., Nef, S., Chaponnier, C., and Vassalli, J.-D. (2011) Beta- and gamma-cytoplasmic actins are required for meiosis in mouse oocytes, *Biol. Reprod.*, **85**, 1025-1039, doi: 10.1095/biolreprod.111.091736.
- Po'uha, S. T., and Kavallaris, M. (2015) Gamma-actin is involved in regulating centrosome function and mitotic progression in cancer cells, *Cell Cycle*, **14**, 3908-3919, doi: 10.1080/15384101.2015.1120920.
- Chen, A., Arora, P. D., McCulloch, C. A., and Wilde, A. (2017) Cytokinesis requires localized β -actin filament production by an actin isoform specific nucleator, *Nat. Commun.*, **8**, 1530, doi: 10.1038/s41467-017-01231-x.
- Sandquist, J. C., Kita, A. M., and Bement, W. M. (2011) And the dead shall rise: actin and myosin return to the spindle, *Dev. Cell*, **21**, 410-419, doi: 10.1016/j.devcel.2011.07.018.
- Uzbekov, R., Kireyev, I., and Prigent, C. (2002) Centrosome separation: respective role of microtubules and actin filaments, *Biol. Cell*, **94**, 275-288, doi: 10.1016/s0248-4900(02)01202-9.
- Lancaster, O., LeBerre, M., Dimitracopoulos, A., Bonazzi, D., Zlotek-Zlotkiewicz, E., Picone, R., Duke, T., Piel, M., and Baum, B. (2013) Mitotic rounding alters cell geometry to ensure efficient bipolar spindle formation, *Dev. Cell*, **25**, 270-283, doi: 10.1016/j.devcel.2013.03.014.
- Rosenblatt, J., Cramer, L. P., Baum, B., and McGee, K. M. (2004) Myosin II-dependent cortical movement is required for centrosome separation and positioning during mitotic spindle assembly, *Cell*, **117**, 361-372, doi: 10.1016/S0092-8674(04)00341-1.

21. Mogessie, B., and Schuh, M. (2017) Actin protects mammalian eggs against chromosome segregation errors, *Science*, **357**, eaal1647, doi: 10.1126/science.aal1647.
22. Jordan, S. N., and Canman, J. C. (2012) Rho GTPases in animal cell cytokinesis: an occupation by the one percent, *Cytoskeleton (Hoboken)*, **69**, 919-930, doi: 10.1002/cm.21071.
23. Chen, X., Wang, K., Svitkina, T., and Bi, E. (2020) Critical roles of a RhoGEF-anillin module in septin architectural remodeling during cytokinesis, *Curr. Biol.*, **30**, 1477-1490.e3, doi: 10.1016/j.cub.2020.02.023.
24. Svitkina, T. (2018) The actin cytoskeleton and actin-based motility, *Cold Spring Harb. Perspect. Biol.*, **10**, a018267, doi: 10.1101/csdperspect.a018267.
25. Piekny, A. J., and Glotzer, M. (2008) Anillin is a scaffold protein that links RhoA, actin, and myosin during cytokinesis, *Curr. Biol.*, **18**, 30-36, doi: 10.1016/j.cub.2007.11.068.
26. Ridley, A. J., and Hall, A. (1992) The small GTP-binding protein Rho regulates the assembly of focal adhesions and actin stress fibers in response to growth factors, *Cell*, **70**, 389-399, doi: 10.1016/0092-8674(92)90163-7.
27. Wagner, E., and Glotzer, M. (2016) Local RhoA activation induces cytokinetic furrows independent of spindle position and cell cycle stage, *J. Cell Biol.*, **213**, 641-649, doi: 10.1083/jcb.201603025.
28. Takaishi, K., Sasaki, T., Kameyama, T., Tsukita, S., Tsukita, S., and Takai, Y. (1995) Translocation of activated Rho from the cytoplasm to membrane ruffling area, cell-cell adhesion sites and cleavage furrows, *Oncogene*, **11**, 39-48.
29. Kosako, H., Yoshida, T., Matsumura, F., Ishizaki, T., Narumiya, S., and Inagaki, M. (2000) Rho-kinase/ROCK is involved in cytokinesis through the phosphorylation of myosin light chain and not ezrin/radixin/moesin proteins at the cleavage furrow, *Oncogene*, **19**, 6059-6064, doi: 10.1038/sj.onc.1203987.
30. Hall, A., and Nobes, C. D. (2000) Rho GTPases: molecular switches that control the organization and dynamics of the actin cytoskeleton, *Philos. Trans. R. Soc. Lond. B Biol. Sci.*, **355**, 965-970, doi: 10.1098/rstb.2000.0632.
31. Halet, G., and Carroll, J. (2007) Rac activity is polarized and regulates meiotic spindle stability and anchoring in mammalian oocytes, *Dev. Cell*, **12**, 309-317, doi: 10.1016/j.devcel.2006.12.010.
32. Dugina, V., Khromova, N., Rybko, V., Blizniukov, O., Shagieva, G., Chaponnier, C., Kopnin, B., and Kopnin, P. (2015) Tumor promotion by γ and suppression by β non-muscle actin isoforms, *Oncotarget*, **6**, 14556-14571, doi: 10.18632/oncotarget.3989.
33. Dugina, V., Shagieva, G., Khromova, N., and Kopnin, P. (2018) Divergent impact of actin isoforms on cell cycle regulation, *Cell Cycle*, **17**, 2610-2621, doi: 10.1080/15384101.2018.1553337.